Synthesis, characterization and crystal structures of two pentagonal-bipyramidal Fe(III) complexes with dihydrazone of 2,6-diacetylpyridine and Girard's T reagent. Anticancer properties of various metal complexes of the same ligand

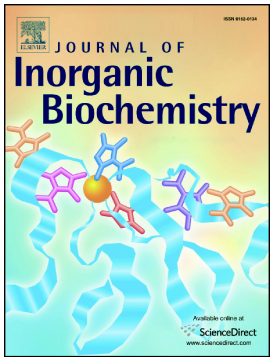

Katarina Anđelković, Milica R. Milenković, Andrej Pevec, Iztok Turel, Ivana Z. Matić, Miroslava Vujčić, Dušan Sladić, Dušanka Radanović, Gabrijela Brađan, Svetlana Belošević, Božidar Čobeljić

PII: S0162-0134(17)30280-5
DOI: doi: 10.1016/j.jinorgbio.2017.06.011
Reference: JIB 10241

To appear in: *Journal of Inorganic Biochemistry*

Received date: 18 April 2017
Revised date: 19 May 2017
Accepted date: 22 June 2017

Please cite this article as: Katarina Anđelković, Milica R. Milenković, Andrej Pevec, Iztok Turel, Ivana Z. Matić, Miroslava Vujčić, Dušan Sladić, Dušanka Radanović, Gabrijela Brađan, Svetlana Belošević, Božidar Čobeljić , Synthesis, characterization and crystal structures of two pentagonal-bipyramidal Fe(III) complexes with dihydrazone of 2,6-diacetylpyridine and Girard's T reagent. Anticancer properties of various metal complexes of the same ligand, *Journal of Inorganic Biochemistry* (2017), doi: 10.1016/j.jinorgbio.2017.06.011

Synthesis, characterization and crystal structures of two pentagonal-bipyramidal Fe(III) complexes with dihydrazone of 2,6-diacetylpyridine and Girard's T reagent. Anticancer properties of various metal complexes of the same ligand.

Katarina Anđelković,[a] Milica R. Milenković,[a] Andrej Pevec,[b] Iztok Turel,[b] Ivana Z. Matić,[c] Miroslava Vujčić,[d] Dušan Sladić,[a] Dušanka Radanović,[d] Gabrijela Brađan,[a] Svetlana Belošević,[e] Božidar Čobeljić[a*]

[a] *Faculty of Chemistry, University of Belgrade, Studentski trg 12-16, Belgrade, Serbia*

[b] *Faculty of Chemistry and Chemical Technology, University of Ljubljana, Večna pot 113, 1000 Ljubljana, Slovenia*

[c] *Institute of Oncology and Radiology of Serbia, Pasterova 14, 11000 Belgrade, Republic of Serbia*

[d] *Institute of Chemistry, Technology and Metallurgy, University of Belgrade, Njegoševa 12, P.O. Box 815, 11000 Belgrade, Serbia*

[e] *Faculty of Technical Sciences, University of Priština, Knjaza Milosa 7, Kosovska Mitrovica, Serbia*

Abstract

In this work synthesis, characterization and crystal structures of two isothiocyanato Fe(III) complexes with 2,2'-[2,6-pyridinediylbis(ethylidyne-1-hydrazinyl-2-ylidene)]bis[*N*,*N*,*N*-trimethyl-2-oxoethanaminium] dichloride (**H$_2$L**Cl$_2$) ligand, with composition [Fe**L**(NCS)$_2$]SCN·2H$_2$O and [Fe**L**(NCS)$_2$]$_2$[Fe(H$_2$O)(NCS)$_5$]·4H$_2$O, has been reported. Both iron(III) complexes possess the same pentagonal-bipyramidal complex cation, while the nature of their anions depends on mole ratio of NH_4SCN and $FeCl_3 \cdot 6H_2O$ used in reaction. Cytotoxic activity of new Fe(III) complexes, as well as of previously synthesized isothiocyanato Co(II), Ni(II), Mn(II), Zn(II) and Cd(II) complexes with the same ligand, was tested against five human

*Email: bozidar@chem.bg.ac.rs

cancer cell lines (HeLa, MDA-MB-453, K562, LS174 and A549) and normal cell line MRC-5. The best activity was observed in the case of Fe(III), Co(II) and Cd(II) complexes. The investigation of potential of these complexes to induce HeLa and K562 cell cycle perturbations was also evaluated. Mechanism of cell death mode was elucidated on the basis of morphological changes of HeLa cells as well as identification of target caspases. It was established that DNA damage could be responsible for the activity of Fe(III) and Co(II) complexes.

Keywords: 2,6-diacetylpyridine dihydrazone, pentagonal-bipyramidal, Fe(III) complexes, crystal structure, cytotoxicity, DNA interactions

1. Introduction

The coordination properties of 2,6-diacetylpyridine bis(acylhydrazones) towards 3d metal ions [1–5], some lanthanides [1, 6–8], main group [1, 9–11], 4d and 5d elements [1] have been intensively studied over the years. The 2,6-diacetylpyridine bis(acylhydrazone) ligands possess at least five donor atoms (N_3O_2) in spatial arrangement which supports formation of seven-coordinated complexes with pentagonal-bipyramidal (PBPY-7) geometry. Pentagonal-bipyramidal geometry is the most common, but not exclusive among the reported complexes with 2,6-diacetylpyridine bis(acylhydrazone) ligands, and possibility for its formation depends on the nature of central metal ion, conformational flexibility of hydrazone ligand and reaction conditions [1]. The acidity of hydrazone function in 2,6-diacetylpyridine bis(acylhydrazone) ligands contributes to structural versatility of their complexes due to possibility of coordination of ligand in non-deprotonated, partially deprotonated and fully deprotonated form [12]. Pentagonal-bipyramidal complexes of 2,6-diacetylpyridine bis(acylhydrazone) ligands have a wide spectrum of biological activities: cytotoxic [11], antimicrobial [9, 10, 13], SOD mimetic [14–16], DNA/RNA binding and nuclease activity [8, 17, 18]. In the previously published papers [19–21], synthesis, characterization and antimicrobial activity of 2,2'-[2,6-pyridinediylbis(ethylidyne-1-hydrazinyl-2-ylidene)]bis[*N*,*N*,*N*-trimethyl-2-oxoethanaminium] dichloride (**H_2L**Cl_2) and its corresponding Mn(II) (**1**), Ni(II) (**2**), Co(II) (**3** and **4**), Zn(II) (**5**) and Cd(II) (**6**) complexes (Scheme 1) were described. In these complexes the ligand **H_2L**Cl_2 is coordinated in non-deprotonated form via pyridine nitrogen, both imine nitrogen and both

carbonyl oxygen atoms. All the complexes possess pentagonal-bipyramidal (PBPY-7) coordination geometry with N_3O_2 coordinated **H₂L**Cl_2 ligand in equatorial plane of the bipyramid and two isothiocyanato ligands in the axial area. The complexes showed a better antimicrobial activity than the ligand. Among the complexes the best activity was observed in the case of Zn(II) (**5**) and Cd(II) (**6**) complexes. As continuation of previous work in this field, in the present paper the syntheses and crystal structures of two isothiocyanato Fe(III) complexes (**7** and **8**) with **H₂L**Cl_2 ligand (Scheme 2) are reported. In order to study the influence of the nature of central metal ion in isothiocyanato PBPY-7 complexes with **H₂L**Cl_2 ligand on their biological activity, antimicrobial and cytotoxic activity of new Fe(III) complexes (**7** and **8**) as well as cytotoxic activity of previously reported Mn(II) (**1**), Ni(II) (**2**), Co(II) (**3** and **4**), Zn(II) (**5**) and Cd(II) (**6**) complexes with **H₂L**Cl_2 ligand were tested.

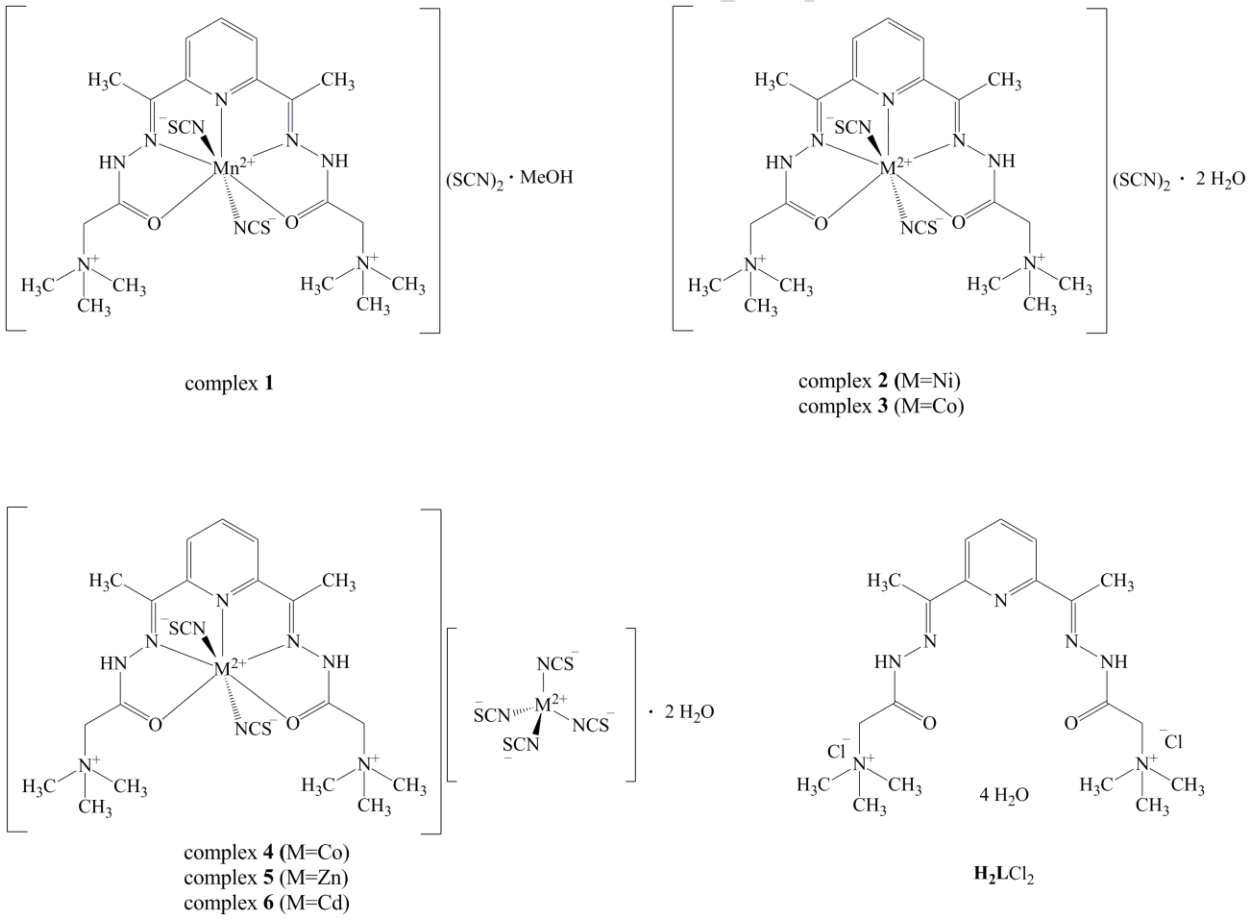

Scheme 1. Pentagonal-bipyramidal isothiocyanato complexes of Mn(II) (**1**), Ni(II) (**2**), Co(II) (**3** and **4**), Zn(II) (**5**) and Cd(II) (**6**) with **H₂L**Cl_2 ligand [19–21]

2. Experimental

2.1. Materials and methods

2,6-Diacetylpyridine (99%) and Girard's T reagent (99%) were obtained from Aldrich. IR spectra were recorded on a Nicolet 6700 FT-IR spectrometer using the ATR technique in the region 4000−400 cm^{-1} (s-strong, m-medium, w-weak). Elemental analyses (C, H, and N) were performed by standard micro-methods using the ELEMENTARVario ELIII C.H.N.S.O analyzer. Molar conductivities were measured at room temperature (25 °C) on a digital conductivity-meter JENWAY-4009.

*2.2. Synthesis of Mn(II) (**1**), Ni(II) (**2**), Co(II) (**3** and **4**), Zn(II) (**5**) and Cd(II) (**6**) complexes*

Pentagonal-bipyramidal isothiocyanato complexes of Mn(II) (**1**), Ni(II) (**2**), Co(II) (**3** and **4**), Zn(II) (**5**) and Cd(II) (**6**) with $\mathbf{H_2L}Cl_2$ ligand were synthesized according to the previously described methods [19−21].

*2.3. Synthesis of [Fe**L**(NCS)$_2$]SCN·2H$_2$O complex (**7**)*

The ligand $\mathbf{H_2L}Cl_2$ (0.25 mmol, 0.13 g) was dissolved in methanol (20 mL) with heating, then $FeCl_3 \cdot 6H_2O$ (0.25 mmol, 0.06 g) and NH_4SCN (1.00 mmol, 0.08g) were added. The solution was heated 3 h at 65 °C. After a few days brownish-red needle-like crystals arose from the reaction solution.

IR: 3501 (m), 3021 (w), 2961 (w), 2055 (s), 1614 (w), 1588 (w), 1542 (m), 1508 (w), 1482 (w), 1402 (m), 1368 (w), 1337 (m), 1273 (w), 1202 (w), 1152 (m), 1123 (w), 1075 (w), 1024 (w), 1001 (w), 970 (w), 920 (w), 808 (w), 736 (w), 677 (w).

Anal. Calcd. for $C_{22}H_{35}FeN_{10}O_4S_3$ (%): C, 40.30; H, 5.38; N 21.36; S, 14.67. Found: C, 39.88; H, 5.52; N, 21.09; S, 14.64.

Λ_M (1 mM, DMSO): 75.0 Ω^{-1} cm^2 mol^{-1}.

*2.4. Synthesis of [Fe**L**(NCS)$_2$]$_2$[Fe(H$_2$O)(NCS)$_5$]·4H$_2$O complex (**8**)*

The ligand **H$_2$L**Cl$_2$ (0.25 mmol, 0.13 g) was dissolved in methanol (20 mL) with heating, then FeCl$_3$·6H$_2$O (0.50 mmol, 0.11 g) and NH$_4$SCN (4.00 mmol, 0.30 g) were added. The solution was heated 3 h at 65 °C. After a few days brownish-red plate crystals arose from the reaction solution.

IR: 3376 (w), 3035 (w), 2040 (s), 1614 (w), 1548 (m), 1479 (w), 1402 (w), 1338 (w), 1270 (w), 1203 (w), 1151 (w), 1073 (w), 1024 (w), 972 (w), 911 (w), 807 (w), 748 (w), 679 (w).

Anal. Calcd. for $C_{47}H_{72}Fe_3N_{23}O_9S_9$ (%): C, 36.20; H, 4.65; N, 20.66; S, 18.50. Found: C, 35.98; H, 4.87; N, 20.53; S, 18.46.

Λ_M (1 mM, DMSO): 136.0 Ω^{-1} cm^2 mol^{-1}.

2.5. X-ray crystal structure determination

Crystal data and refinement parameters of compounds **7** and **8** are listed in Table S1 (see Supplementary Information). The X–ray intensity data were collected at 150 K with Agilent SuperNova dual source with Atlas detector equipped with mirror–monochromated Mo–K_α radiation (λ = 0.71073 Å). The data were processed using CRYSALIS PRO [22]. Both structures were solved by direct methods using SIR-92 [23] and refined against F^2 on all data by a full-matrix least squares procedure with SHELXL-97 [24]. All non-hydrogen atoms were refined anisotropically. All of the C–H hydrogen atoms were included in the model at geometrically calculated positions and refined using a riding model. The hydrogen atoms bonded to water oxygen atoms were visible in the last stages of the refinement and were refined with the constrained O–H bond length (0.96 Å) and isotropic thermal parameters (1.5 times the thermal parameter of the attached oxygen atom). The residual density peak in **8** (3.01 Å from C41) was unrefinable and therefore was not included in the model. The sulfur atoms in **8** bonded to C20, C21 and C44 of SCN$^-$ ligands are disordered over two orientations and were modelled with split positions, with the use of PART instruction. Crystallographic data for structures have been deposited at the Cambridge Crystallographic Data Centre as supplementary publication CCDC 1543583 and 1543584 for **7** and **8**, respectively. Copies of the structures can be obtained free of charge www.ccdc.cam.ac.uk/data_request/cif.

2.6. Antimicrobial activity

Antimicrobial activity of compounds was tested by the broth-microdilution method according to the procedure prescribed by the CLSI (Clinical and Laboratory Standards Institute) [25] against seven standard strains of bacteria and one strain of yeast *Candida albicans (C. Albicans).* The compounds were dissolved in distilled water and tested within the concentration range of 1000 μg/mL to 62.5 μg/mL. Antibiotic gentamicin and ciprofloxacin were used as a control for bacteria and amphotericin was used for *C. albicans*. All tests were performed in Müller-Hinton broth for the bacterial strains and in Sabouraud dextrose broth for *C. albicans*. All of the MIC determinations were performed in duplicate, and two positive growth controls were included.

2.7. Cytotoxic activity

The cytotoxic activities of the complexes and their precursor compounds were examined on five human cancer cell lines: cervical adenocarcinoma HeLa, breast carcinoma MDA-MB-453, chronic myelogenous leukemia K562, colon adenocarcinoma LS174, lung carcinoma A549, and normal human lung fibroblasts MRC-5, as described elsewhere [26]. All tested cell lines were obtained from the American Type Culture Collection (Manassas, VA, USA). HeLa (2,000 cells per well), MDA-MB-453 (3,000 cells per well), LS174 (7,000 cells per well), A549 (5,000 cells per well) and MRC-5 (5,000 cells per well) were seeded into 96-well microtiter plates and 20 h later the adherent cells were treated with five different concentrations of the tested compounds (ranging from 12.5 μM to 200 μM). Nutrient medium only was added to the control cell samples. K562 cells (5,000 cells per well) were seeded 2 h before the treatment with compounds. Stock solutions of the seven complexes (**2**–**8**) were prepared in DMSO at a concentration of 10 mM, while stock solutions of tested precursors and complex **1**, were prepared in a sterile water at a concentration of 10 mM. The final DMSO concentration did not affect cell survival. Cell survival was determined by MTT assay after 72 h of continual treatment, according to the method of Mosmann [27], which was modified by Ohno and Abe [28] and described previously [26].

Chemotherapy drug cisplatin was used as a positive control in all experiments.

2.8. Cell cycle analysis by flow cytometry

HeLa and K562 cells were treated with IC_{50} and $2IC_{50}$ concentrations of the complexes **4**, **6** and **8** (the applied concentrations were determined after 72 h treatment for each complex) for 24 h. After treatment, the cells were collected, washed and fixed in 70 % ethanol, according to standard procedure [26, 29]. Cisplatin was used as a positive control. Cell cycle phase distributions were determined using a FACSCalibur flow cytometer (BD Biosciences, Franklin Lakes, NJ, USA). The analyses of acquired data (10,000 events collected for each gated cell sample) were performed using a CELLQuest software (BD Biosciences). Cell cycle distribution data are presented as mean±S.D. of three independent experiments. The statistical significance of differences between the control and treated cell samples was evaluated using one-way ANOVA with Dunnett's post test. *p* values below 0.05 were considered statistically significant.

2.9. Fluorescence microscopy

To examine the mode of cell death induced by the complexes **4**, **6** and **8**, morphological analysis by fluorescence microscopy of HeLa cells stained with a mixture of acridine orange and ethidium bromide was performed, according to previously described protocol [26]. Cisplatin was used as a positive control. The visualization was done using Carl Zeiss PALM MicroBeam microscope with Axio Observer.Z1 and AxioCam MRm camera (filters: Alexa 488 and Alexa 568).

2.10. Determination of target caspases

To explore whether complexes **4**, **6** and **8** could induce apoptosis in HeLa cells, the percentages of subG1 cells in the samples pretreated with caspase inhibitors were determined, as previously described by Matić *et al*. [26]. The specific caspase inhibitors applied at concentration of 40 μM were: Z-DEVD-FMK, a caspase-3 inhibitor, Z-IETD-FMK, a caspase-8 inhibitor and Z-LEHD-FMK, a caspase-9 inhibitor (R&D Systems, Minneapolis, USA).

2.11. Tube formation assay

The possible antiangiogenic effects of the complexes **4**, **6** and **8** were examined on human umbilical vein EA.hy926 cell line using endothelial cell tube formation assay [30,31]. The EA.hy926 cells seeded on Corning® Matrigel® basement membrane matrix (Corning: cat. number 356234) were treated with sub-toxic IC_{20} concentrations of the complexes **4**, **6** and **8** (200 µM, 50 µM and 50 µM respectively) for 20 h. Photomicrographs of EA.hy926 cells were captured under the inverted phase-contrast microscope.

2.12. DNA binding experiments

Calf thymus DNA (lyophilized, highly polymerized, obtained from Serva, Heidelberg) (CT-DNA) was dissolved in Tris buffer (10 mM Tris-HCl pH 7.9) overnight at 4 °C. This stock solution was stored at 4 °C and was stable for several days. A solution of CT-DNA in water gave a ratio of UV absorbance at 260 and 280 nm, A_{260}/A_{280} of 1.89–2.01, indicating that DNA was sufficiently free of protein. The concentration of DNA (2.86 mg mL^{-1}) was determined from the UV absorbance at 260 nm using the extinction coefficient ε_{260}=6600 M^{-1} cm^{-1} [32]. The complexes of Co(II) (**4**), Cd(II) (**6**) and Fe(III) (**8**) were dissolved in dimethyl sulfoxide in concentrations of 10 mM. These solutions were used as stock solutions.

2.12.1. Absorption spectral measurements

For an UV-Vis measurement, a small volume of a stock solution of the complex of different concentrations was added to DNA solution (10 µL of CT-DNA) and the volume was adjusted up to 1 mL with 40 mM bicarbonate buffer, pH 8.4. Reaction mixtures were incubated at 37 °C for 90 min with occasional vortexing. UV–Vis spectra were recorded on a UV-1800 Shimadzu UV/Visible spectrophotometer operating from 200 to 800 nm in 1.0 cm quartz cells. Spectra of the complexes of the same concentrations were also recorded, as well as spectra of CT-DNA. The absorbance titrations were performed at a fixed concentration of the complex and gradually increasing concentration of double stranded CT-DNA. The absorbance at 259 nm was monitored for each concentration of DNA. The binding constant K_b was determined using the equation (1) [33]:

$$[DNA] \times (\varepsilon_a - \varepsilon_f)^{-1} = [DNA] \times (\varepsilon_b - \varepsilon_f)^{-1} + K_b^{-1} \times (\varepsilon_b - \varepsilon_f)^{-1}, \qquad (1)$$

where ε_a, ε_f, ε_b are absorbance/[complex], extinction coefficient of the free complex and the extinction coefficient of the bound complex, respectively. A plot of [DNA]/($\varepsilon_a - \varepsilon_f$) *versus* [DNA] gave a slope and the intercept equal to $1/(\varepsilon_a - \varepsilon_f)$ and $(1/K_b)(1/(\varepsilon_b - \varepsilon_f))$, respectively. The binding constant K_b is calculated from the ratio of the slope to the intercept.

2.12.2. Fluorescence measurements

The competitive interactions of complexes **4**, **6** and **8** and the fluorescence probe either ethidium bromide (EB) or Hoechst 33258 (H), with CT-DNA have been studied by measuring the change of fluorescence intensity of the probe−DNA solution after addition of the complex. Reaction mixtures containing 100 µM of CT-DNA (calculated per phosphate) in 1 mL of 40 mM bicarbonate solution (pH 8.4) were pretreated with 1.5 µL of 1% H probe solution (28 µM final concentration) or 1 µL of 1% EB solution (25 µM final concentration) (in separate experiments) for 20 min and the mixture was analyzed by fluorescence measurement. Then the increasing concentrations of the complexes were successively added and the changes in the fluorescence intensity were measured using a Thermo Scientific Lumina Fluorescence spectrometer (Finland) equipped with a 150 W Xenon lamp. The slits on the excitation and emission beams were fixed at 10 nm. All measurements were performed by excitation at 350 nm for Hoechst 33258, and by excitation at 500 nm for EB in the range of 390−600 nm. The control was probe−CT-DNA solution. Complexes of Co(II) (**4**), Cd(II) (**6**) and Fe(III) (**8**) did not have fluorescence under applied conditions. The obtained fluorescence quenching data were analyzed according to the Stern–Volmer equation (2) [34]:

$$I_0/I = 1 + K\boldsymbol{r} \qquad (2)$$

where I_0 and I represent the fluorescence intensities of probe−CT-DNA in absence and presence of the complex, respectively, K is quenching constant. The K value is calculated from the ratio of the slope to the intercept from the plot of I_0/I *versus* $\boldsymbol{r}$ ($\boldsymbol{r}$ = [complex]/[CT-DNA].

Primary spectra of all spectrometric measurements were imported into OriginPro 8.0 and were processed by this software package.

2.12.3. DNA cleavage experiments

For DNA cleavage experiments the plasmid pUC19 (2686 bp, purchased from Sigma-Aldrich, USA) was prepared by its transformation in chemically competent cells *Escherichia coli* (*E. coli*) strain XL1 blue. Amplification of the clone was done according to the protocol for growing *E. coli* culture overnight in LB medium at 37 °C [35] and purification was performed using Qiagen Plasmid plus Maxi kit. Finally, DNA was eluted in 10 mM Tris-HCl buffer and stored at −20 °C. The concentration of plasmid DNA (512 ng μL^{-1}) was determined by measuring the absorbance of the DNA-containing solution at 260 nm. One optical unit corresponds to 50 μg mL^{-1} of double stranded DNA.

The cleavage reaction of supercoiled pUC19 DNA with different concentration of **4**, **6** and **8** was investigated by incubation of 460 ng of plasmid in a 20 μL reaction mixture in 40 mM bicarbonate buffer (pH 8.4) at 37 °C, for 90 minutes. The reaction mixtures were vortexed from time to time. The reaction was terminated by short centrifugation at 10000 rpm and addition of 5 μL of loading buffer (0.25% bromophenol blue, 0.25% xylene cyanol FF and 30% glycerol in TAE buffer, pH 8.24 (40 mM Tris-acetate, 1 mM EDTA)).

2.12.4. Agarose electrophoresis

The samples were subjected to electrophoresis on 1% agarose gel (Amersham Pharmacia-Biotech, Inc) prepared in TAE buffer pH 8.24. The electrophoresis was performed at a constant voltage (80 V) until bromophenol blue had passed through 75% of the gel. A Submarine Mini-gel Electrophoresis Unit (Hoeffer HE 33) with an EPS 300 power supply was used. After electrophoresis, the gel was stained for 30 min by soaking it in an aqueous ethidium bromide solution (0.5 μg mL^{-1}). The stained gel was illuminated under a UV transilluminator Vilber-Lourmat (France) at 312 nm and photographed with a Nikon Coolpix P340 Digital Camera through filter DEEP YELLOW 15 (TIFFEN, USA).

3. Results and discussion

3.1. Synthesis

Pentagonal-bipyramidal isothiocyanato complexes of Mn(II) (**1**), Ni(II) (**2**), Co(II) (**3** and **4**), Zn(II) (**5**) and Cd(II) (**6**) with 2,2'-[2,6-pyridinediylbis(ethylidyne-1-hydrazinyl-2-ylidene)]bis[*N*,*N*,*N*-trimethyl-2-oxoethanaminium] dichloride (**H$_2$L**Cl$_2$) (Scheme 1) were synthesized according to the previously reported methods [19−21]. Iron(III) complexes **7** and **8** were obtained in the reaction of the ligand **H$_2$L**Cl$_2$, $FeCl_3 \cdot 6H_2O$ and NH_4SCN (Scheme 2). The complexes possess the same pentagonal-bipyramidal complex cation, while the nature of their anions depends on mole ratio of NH_4SCN and $FeCl_3 \cdot 6H_2O$ used in reaction. The complexes were characterized by elemental analysis, IR spectroscopy, conductometric measurements and X-ray analysis. The observed value of molar conductivity for complex **7** corresponds to 1:1 electrolyte indicating stability of PBPY-7 complex cation in solution. The value of molar conductivity for complex **8** indicates solvolysis of complex anion $[Fe(H_2O)(NCS)_5]^{2-}$ whereby one or two coordinated SCN^- ligands are replaced with molecules of solvent [36].

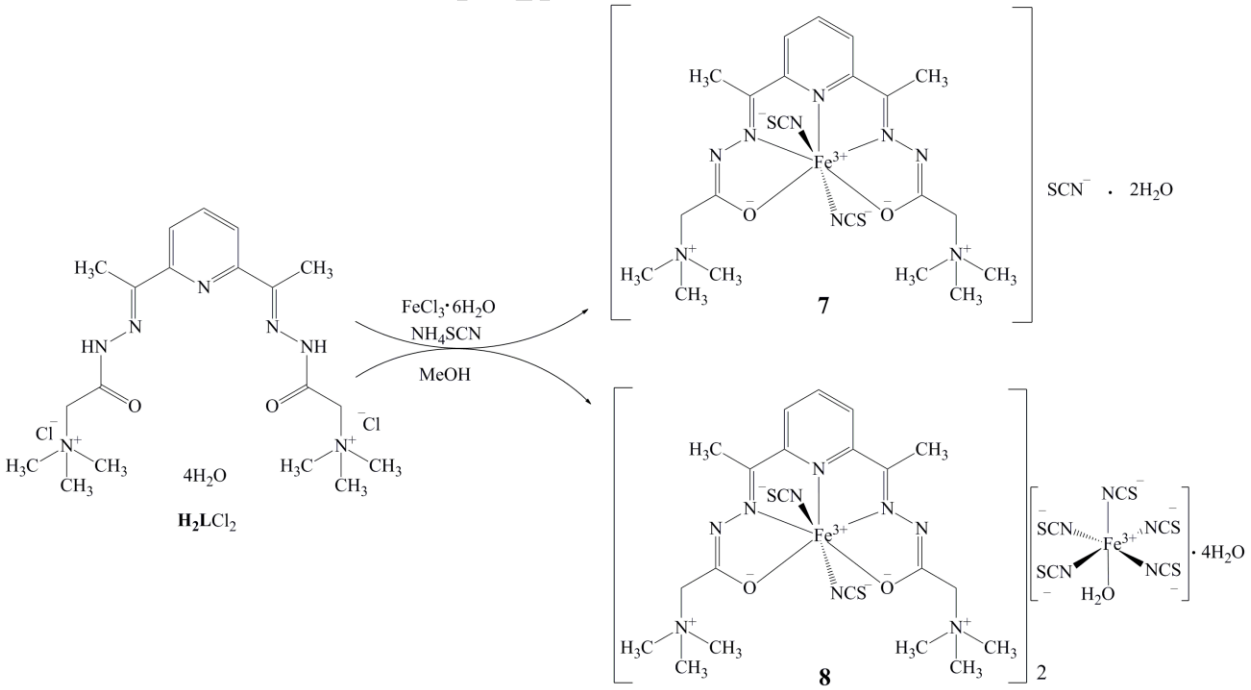

Scheme 2. Synthesis of Fe(III) complexes **7** and **8**.

3.2. Spectroscopy

Comparison of IR spectra of $\mathbf{H_2L}Cl_2$ and complexes **7** and **8** indicates symmetric coordination of deprotonated bishydrazone ligand. In the IR spectra of complexes **7** and **8** a band corresponding to ν(O–C=N) of the deprotonated ligand appeared at 1614 cm^{-1} instead of the carbonyl band from uncoordinated ligand at 1707 cm^{-1} [37]. Coordination of azomethine nitrogen atoms results in bathochromic shift of the ν(C=N) band from 1630 cm^{-1} in the spectrum of $\mathbf{H_2L}Cl_2$ to 1588 cm^{-1} in the spectra of complexes **7** and **8** [37]. In the IR spectra of complexes **7** and **8** broad strong bands at 2055 cm^{-1} and 2040 cm^{-1}, respectively, originate from N-coordinated thiocyanate anions [38].

3.4. Crystal structures

Both compounds **7** and **8** crystallized in triclinic crystal system with space group *P*-1. Selected bond lengths and angles are listed in Table S2. ORTEP representations of the structures are given in Figures 1 and 2. The major building unit in crystal structures of both compounds is complex cation where Fe(III) ion is coordinated by ligand **L** and two SCN^- ligands forming distorted pentagonal-bipyrimidal coordination geometry. Four fused five-membered chelate rings are formed during coordination of pentadentate ligand to Fe(III) ion. In compound **7**, the counter ion of cationic $[Fe\mathbf{L}(NCS)_2]^+$ complex is SCN^- anion. There are also two solvate water molecules per complex cation in the crystal structure. The asymmetric unit of compound **8** consists of two complex cations $[Fe\mathbf{L}(NCS)_2]^+$ per one $[Fe(H_2O)(NCS)_5]^{2-}$ anion and four uncoordinated water molecules. In the solid state structure of both compounds **7** and **8** cations, anions and uncoordinated water molecules are connected by O–H···N and O–H···O hydrogen bonds. Complex cations $[Fe\mathbf{L}(NCS)_2]^+$ in **7** form dimers through the C-H···π type interactions (H7B···Cg distance is 2.83 Å, where Cg is the center of gravity of the pyridine ring at –x, –y, 1–z). The coordination geometry of cationic complex $[Fe\mathbf{L}(NCS)_2]^+$ is close to other complexes with pentagonal-bipyramidal geometry and N_3O_2 donor sets of ligand $\mathbf{H_2L}^{2+}$ [19–21]. Only the distances Fe–O in **7** and **8** are slightly shorter than in other $[M\mathbf{H_2L}(SCN)_2]^{2+}$ complexes. The

complex anion $[Fe(H_2O)(NCS)_5]^{2-}$ was also found in $(C_6H_6NO_2)_2[Fe(NCS)_5(H_2O)]\cdot 2C_6H_5NO_2$ [39] the only known example of complex anion $[Fe(H_2O)(NCS)_5]^{2-}$ found in the crystal structure [40].

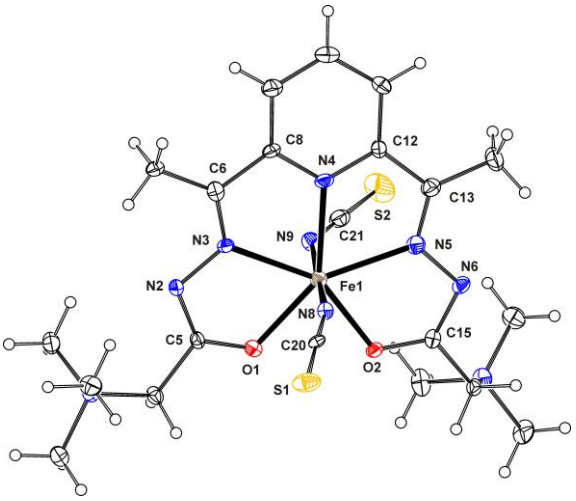

Figure 1. ORTEP plot of **7** with thermal ellipsoids at 30 % probability level. Hydrogen atoms, water molecules and uncoordinated SCN^- ligand are omitted for clarity.

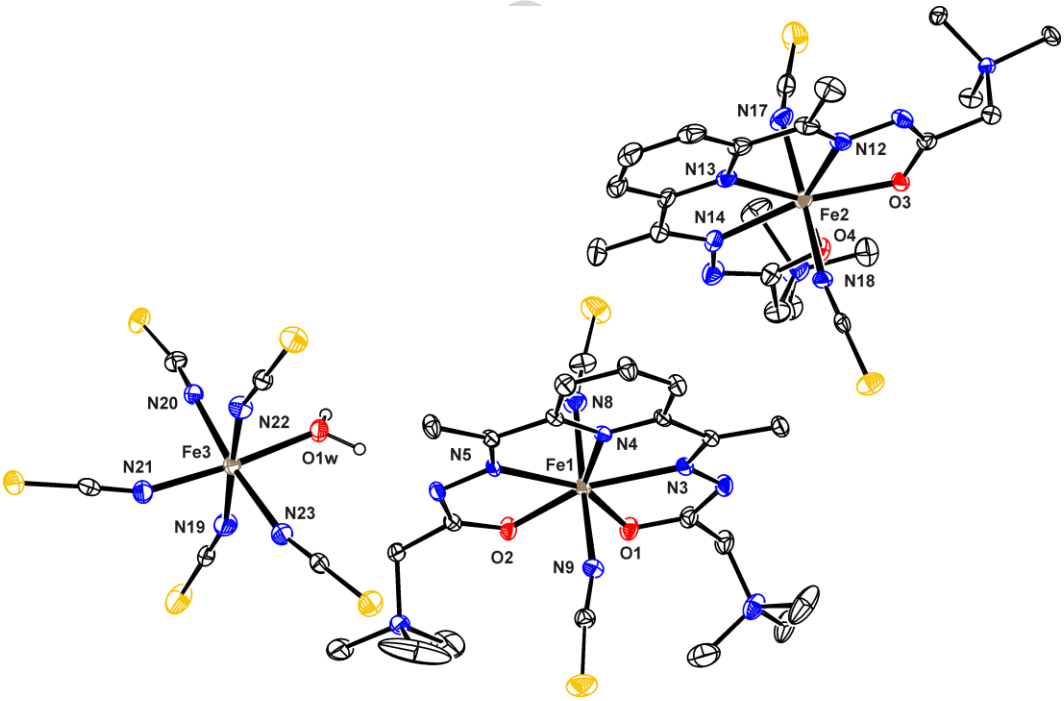

Figure 2. ORTEP plot of **8** with thermal ellipsoids at 30 % probability level. Hydrogen atoms bonded to carbon atoms and uncoordinated water molecules are omitted for clarity.

3.5. Antimicrobial activity

The results of antimicrobial activity for Fe(III) complexes **7** and **8** are presented in Table 1. Both complexes showed better activity than the ligand **H$_2$L**Cl$_2$ and FeCl$_3$·6H$_2$O, but their MIC values were higher than the values for standard antimicrobial agents. Complex **8** exhibited moderate activity against all the tested microbial strains. The activity of complex **7** was low to moderate. The highest activity of both complexes was observed against *B. subtilis*. Complexes **8** and **7** showed better activity against Gram positive than Gram negative bacterial strains. Among the investigated compounds only complex **8** exhibits moderate activity against *C. albicans*. Amount of pentagonal-bipyramidal complex cation per mole of compound is twice higher in **8** than in **7**, but MIC values for complex **7** are not twice of the values for complex **8**, indicating that the nature of their anions (SCN^- in the case of compound **7** and $[Fe(H_2O)(NCS)_5]^{2-}$ in the case of compound **8**) also influence antimicrobial activity. In biological systems peroxidase catalyzed SCN^- oxidation by endogenous H_2O_2 results in formation of hypothiocyanite ($OSCN^-$), which possesses antimicrobial activity. Antimicrobial activity of hypothiocyanite is attributed to its reaction with sulfhydryl groups of glycolytic enzymes and thiol-based antioxidants [41]. Also, hypothiocyanite is the product of non-catalysed oxidation of thiocyanate by hydrogen peroxide [42] or ferric ion [43]. In aqueous solution isothiocyanato ligands of complex anion $[Fe(H_2O)(NCS)_5]^{2-}$ are displaced by water molecules [43]. Free SCN^- can be oxidized to hypothiocyanite by H_2O_2 produced in oxidative metabolism of aerobic prokaryotic cells. Also, Fe(III) complex species originating from $[Fe(H_2O)(NCS)_5]^{2-}$ can oxidize SCN^- to $OSCN^-$ with formation of ferrous species. Fenton reaction [44] of Fe^{2+} with H_2O_2 generates hydroxyl radicals which have a strong non-selective antimicrobial activity. The fact that complexes **7** and **8** showed better activity towards Gram positive than Gram negative bacteria, indicates that their antibacterial activity depends on the structural features of the bacterial cell wall. Iron(III) complexes **7** and **8** showed better antimicrobial activity than pentagonal-bypiramidal isothiocyanato Ni(II), Co(II), Zn(II) and Cd(II) complexes [20, 21] with the same bis(acylhydrazone) ligand.

Table 1. Antimicrobial activity of ligand **H_2L**Cl_2 and complexes **7** and **8**, MIC (mM).

Microorgamisms	**H_2L**Cl_2	$FeCl_3 \cdot 6H_2O$	**7**	**8**	Gentamicin	Ciprofloxacin	Amphotericin
S. aureus ATCC 6538	1.876	>3.699	1.527	0.160	n.t.	0.001	n.t.
S. epidermidis ATCC 1228	0.938	>3.699	0.382	0.160	0.002	0.002	n.t.
B. subtilis ATCC 6633	0.938	>3.699	0.382	0.080	0.001	0.002	n.t.
E. coli ATCC 10536	1.876	>3.699	0.382	0.160	0.001	0.001	n.t.
K. pneumoniae ATCC 13883	>1.876	>3.699	1.527	0.321	0.008	0.002	n.t.
P. aeruginosa ATCC 9027	>1.876	>3.699	>1.527	0.321	0.005	0.002	n.t.
S. enterica NCTC 6017	>1.876	>3.699	>1.527	0.321	0.002	0.002	n.t.
C. albicans ATCC 10231	>1.876	>3.699	1.527	0.642	n.t.	0.001	0.003

n.t. – not tested

3.7. Cytotoxic activity

The examined compounds showed concentration-dependent moderate to low cytotoxic activities on five tested human cancer cell lines, as well as on normal, non-transformed human fibroblasts MRC-5, as presented in Table 2. The cytotoxic activities of the tested complexes were lower against all malignant cell lines in comparison with the activity of cisplatin, which served as a positive control. The complexes **4**, **6** and **8** exerted the most pronounced selective cytotoxic effects on all examined cancer cell lines. Human myelogenous leukemia K562 cells were the most sensitive to complex **4** with IC_{50} value of 38.66 μM and complex **8** with IC_{50} value of 48.33 μM. Breast carcinoma MDA-MB-453 cells had the highest sensitivity to the cytotoxic activity of complex **6**, which also exerted the most pronounced cytotoxicity against this cell line with IC_{50} value of 59.40 μM. The complexes **4** and **8** also showed pronounced cytotoxic activity on MDA-MB-453 cells with IC_{50} values of 76.51 and 87.27 μM, respectively. Human cervical adenocarcinoma HeLa cells were the most sensitive to the cytotoxic effects of complexes **4** and **6** with IC_{50} values of 70.46 and 71.06 μM, respectively; while complex **8** exerted slightly lower activity on HeLa cells with IC_{50} 106.61 μM. Lung carcinoma A549 cells exerted sensitivity to the action of complexes **4**, **6** and **8** with IC_{50} values of 79.53, 84.76 and 70.45 μM, respectively. The examined complexes did not show selectivity in the cytotoxic activity against cancer cell lines in comparison with non-transformed normal lung fibroblasts MRC-5, exerting pronounced cytotoxic effects on MRC-5 cells. Complex **6** showed higher activity against A549 cells and lower toxicity against normal MRC-5 cell line than Cd(II) salt. Cobalt complex **3** with free thiocyanate anion exhibited lower cytotoxic activity than cobalt complex **4** with complex anion $[Co(NCS)_4]^{2-}$ and cobalt(II) salt. The activity of complex **4** is higher than the activity of cobalt(II) salt. Better activity of complex **4** can be attributed to synergistic effect of PBPY-7 complex cation and $[Co(H_2O)_6]^{2+}$ formed from $[Co(NCS)_4]^{2-}$ which has low stability in water solution [20].

Table 2. The cytotoxic activity of the investigated complexes and its precursors.

	HeLa	**MDA-MB-453**	**K562**	**LS174**	**A549**	**MRC-5**
	IC_{50} [μM] *mean±S.D.*					
1	187.28±18.91	183.33±23.57	190.93±15.71	>200	187.66±21.38	198.35±2.86
2	186.85±22.77	187.85±17.18	194.51±7.76	170.82±33.19	144.42±7.69	46.79±1.52

3	96.75±11.82	135.01±1.55	76.99±10.54	176.90±11.44	129.77±28.30	92.08±7.82
4	70.46±13.59	76.51±17.69	38.66±3.49	115.25±28.19	79.53±14.47	54.57±14.24
5	190.10±17.15	111.37±4.74	122.80±0.30	170.72±41.42	130.85±5.77	121.78±14.49
6	71.06±5.95	59.40±14.21	72.98±6.10	160.46±16.44	84.76±3.08	86.89±13.94
7	110.98±24.45	115.69±7.86	75.94±5.20	171.84±34.78	98.72±1.55	80.42±0.06
8	106.61±15.92	87.27±4.06	48.33±6.87	116.11±31.00	70.45±7.60	40.19±0.73
H_2LCl_2	>200	>200	>200	>200	>200	>200
$MnCl_2 \cdot 4H_2O$	156.84±38.49	138.40±30.35	85.07±21.12	192.67±12.70	189.62±7.17	143.62±23.04
$NiCl_2 \cdot 6H_2O$	76.31±1.09	111.59±2.08	77.76±2.91	136.61±28.97	127.68±27.82	78.75±15.03
$CoCl_2 \cdot 6H_2O$	95.37±9.56	92.01±12.11	45.73±3.57	136.79±0.45	97.98±12.81	57.58±1.98
$ZnCl_2 \cdot 2H_2O$	>200	191.32±12.27	169.87±28.50	>200	200.00±0.00	105.61±25.82
$Cd(NO_3)_2 \cdot 4H_2O$	79.16±1.62	56.40±11.08	49.16±13.70	112.57±22.16	126.80±15.25	57.27±14.68
$FeCl_3 \cdot 6H_2O$	>200	>200	>200	>200	>200	>200
cisplatin	4.73±0.88	6.05±1.12	5.63±0.21	24.86±3.41	9.43±0.60	8.56±1.58

3.8. Changes in the cell cycle phase distribution

To explore the mechanisms of cytotoxic effects of the most active complexes **4**, **6** and **8**, cell cycle analysis of HeLa and K562 cells treated with IC_{50} and $2IC_{50}$ concentrations of these compounds for 24 h was performed. The changes in the cell cycle phase distribution of these cells induced by the chosen compounds are presented in Figure 3. Treatment of HeLa cells with IC_{50} and $2IC_{50}$ concentrations of complex **6** induced a statistically significant increase of HeLa cells in subG1 cell cycle phase and significant decrease of cells in G2/M phase when compared with control untreated cells. The exposure of HeLa cells to complexes **4** and **8** applied at $2IC_{50}$ concentrations led to significant increase in the percentage of subG1 cells in addition to significantly reduced percentage of cells in S phase in comparison with control cell sample. Furthermore, complexes **4** and **8** caused accumulation of HeLa cells in G1 cell cycle phase, although the observed change was not statistically significant. Cisplatin applied at $2IC_{50}$ concentration caused increase in subG1 and S phases and decrease G2/M phase of cell cycle in HeLa cells. The complex **6** applied at IC_{50} and $2IC_{50}$ concentrations for 24 h caused G1 cell cycle phase arrest in K562 cells, which was statistically significant when compared with untreated cells. The accumulation of K562 cells in G1 phase treated with $2IC_{50}$ concentration of complex **6**

was accompanied with significant increase of cells within subG1 phase in addition to significantly decreased percentage of cells within S and G2/M phases. Treatment of K562 cells with $2IC_{50}$ concentration of complex **4** induced significant increase of cells in G1 phase and significant decrease of cells in S and G2/M cell cycle phases in comparison with control K562 cells. Cisplatin applied at $2IC_{50}$ concentration caused increase in subG1 and G1 phases and decrease in S and G2/M phases of cell cycle in K562 cells.

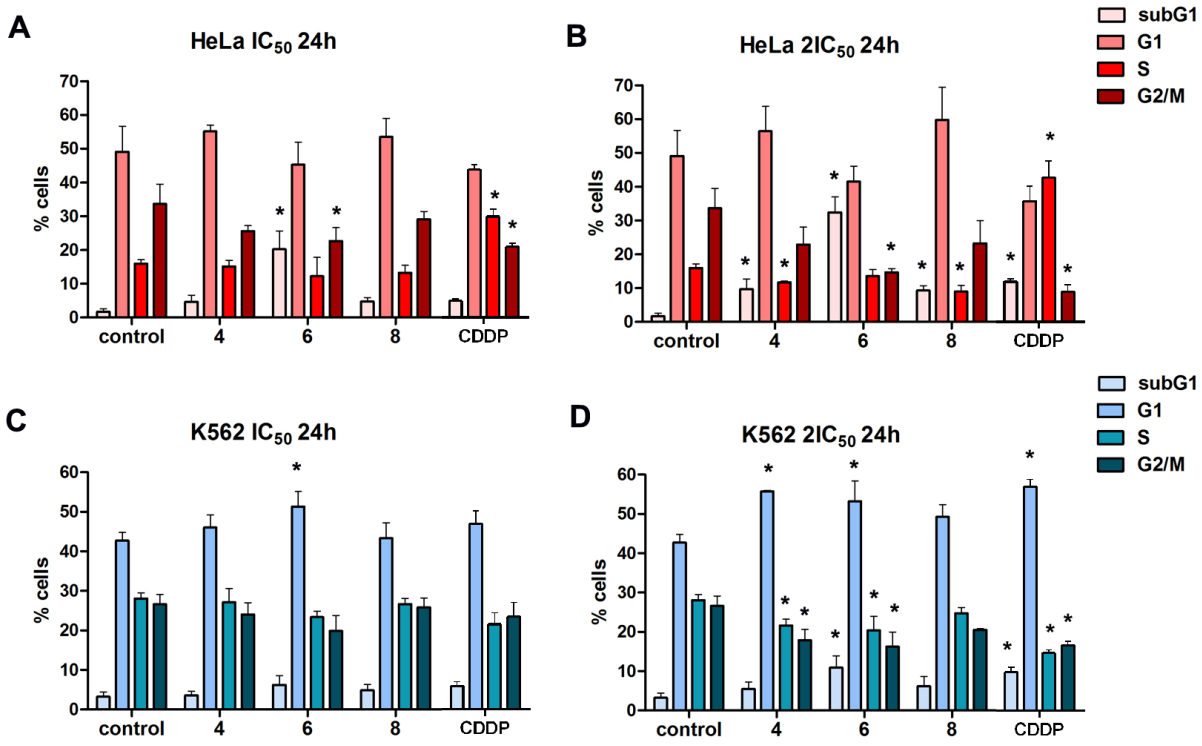

Figure 3. Changes in the cell cycle phase distribution of HeLa (A, B) and K562 cells (C, D) treated with IC_{50} and $2IC_{50}$ concentrations of complexes **4**, **6** and **8**, and cisplatin (CDDP). The results are presented as the mean ± S.D. from three independent experiments. Statistically significant differences between control and treated cells are marked with * ($p<0.05$). Applied IC_{50} concentrations of the tested compounds were: 70.46, 71.06, 106.61 and 4.73 µM, respectively for HeLa cells and 38.66, 72.98, 48.33 and 5.63 µM, respectively for K562 cells.

3.9. Morphological evaluation of HeLa cell death mode

The examination of morphological changes of HeLa cells treated for 24 h with $2IC_{50}$ concentrations of complexes **4**, **6** and **8** demonstrated the ability of these compounds to trigger apoptosis in HeLa cells (Figure 4). The pro-apoptotic effect of complex **6** was more pronounced in HeLa cells when compared with the effects of complexes **4** and **8**, as showed by cell cycle analysis as well. Typical morphological hallmarks of apoptosis could be observed in HeLa cells incubated with tested complexes, such as rounded cells, shrinkage of the nucleus, chromatin condensation and fragmentation of the nucleus in addition to orange-red stained HeLa cells in the later stages of apoptosis. Morphological characteristics of apoptosis were also observed in HeLa cells exposed to cisplatin.

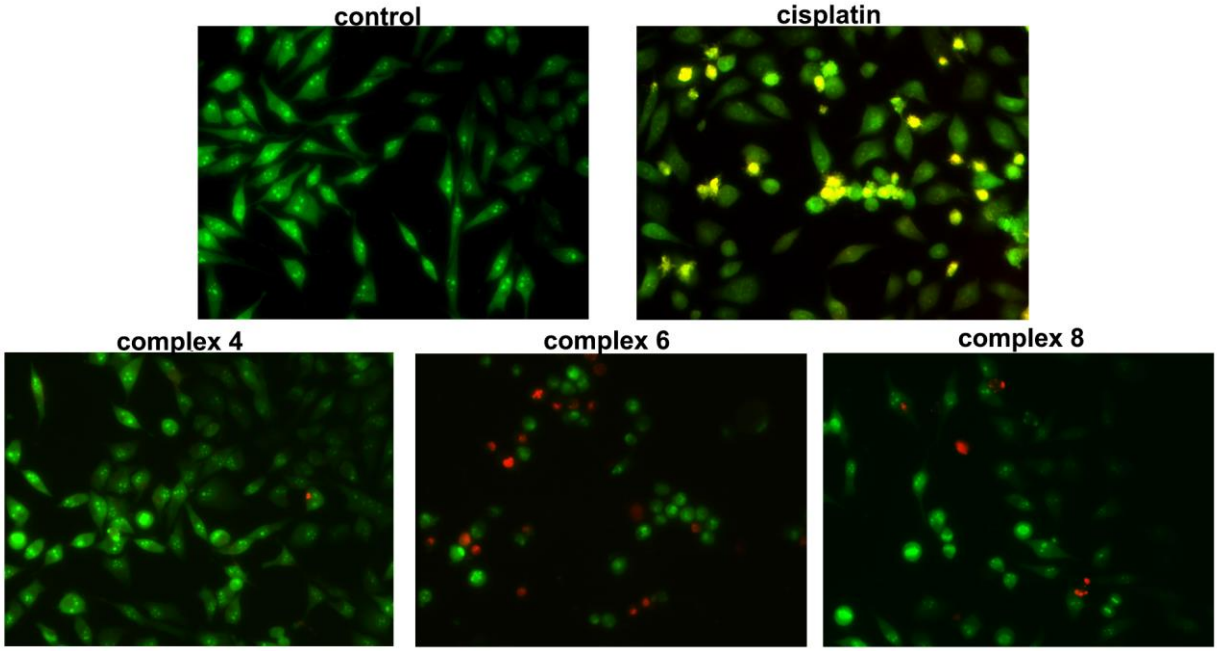

Figure 4. Photomicrographs of acridine orange/ethidium bromide-stained control HeLa cells and HeLa cells exposed to $2IC_{50}$ concentrations of the cisplatin (9.46 μM) and complexes **4**, **6** and **8** (140.92, 142.12 and 213.22 μM, respectively) for 24 h.

3.10. Identification of target caspases

To further elucidate the mechanisms of the cell death mode induced by the complexes **4**, **6** and **8** in HeLa cells, the effects of the pretreatment with specific inhibitors of caspase-3, caspase-8 and caspase-9 were examined by cell cycle analysis (Figure 5). Decrease in the percentage of HeLa

cells within subG1 phase was observed in the samples exposed to complexes **4** and **8** and pretreated with the inhibitors of caspase-3, caspase-8 or caspase-9, when compared with the percentages of HeLa cells in subG1 phase in the samples which were not pretreated with these specific inhibitors. Treatment with complex **6** of HeLa cells pretreated with inhibitors of caspase-3 or caspase-9 led to remarkable decrease of subG1 cells in comparison with cells which were not pre-exposed to inhibitors before treatment with complex **6**. However, the pretreatment with caspase-8 inhibitor did not reduce the percentage of subG1 cells incubated with this complex. Our results point out that complexes **4** and **8** possess the ability to trigger extrinsic and intrinsic apoptotic signaling pathways in HeLa cells. The complex **6** induces prominent pro-apoptotic effect in HeLa cells through intrinsic apoptotic pathway. The effects of caspase-3 and caspase-9 inhibitors on the activity of complex **6** in HeLa cells may suggest that this complex could activate caspase-independent apoptosis or other cell death types besides apoptosis.

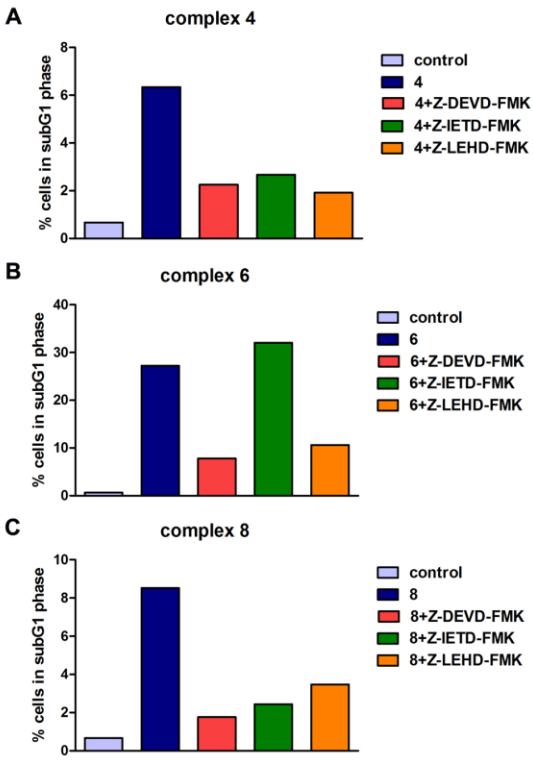

Figure 5. Effects of the specific caspase inhibitors (Z-DEVD-FMK - caspase-3 inhibitor; Z-IETD-FMK -caspase-8 inhibitor; Z-LEHD-FMK - caspase-9 inhibitor) on the percentages of subG1 HeLa cells treated with $2IC_{50}$ concentrations of the complexes **4** (A), **6** (B) and **8** (C) (140.92, 142.12 and 213.22 μM, respectively).

3.11. Effects on the in vitro angiogenesis

The endothelial cell tube formation assay showed weak suppressive effects of complexes **4**, **6** and **8** applied at sub-toxic IC_{20} concentrations (200, 50 and 50 μM, respectively) on *in vitro* angiogenesis of EA.hy926 cells (Figure 6). Each of the tested complexes showed the ability to inhibit formation of capillary-like tube structures, observed in the control, untreated EA.hy926 cells. The antiangiogenic effects of complexes **6** and **8** were to some extent more pronounced when compared with the effect of complex **4**.

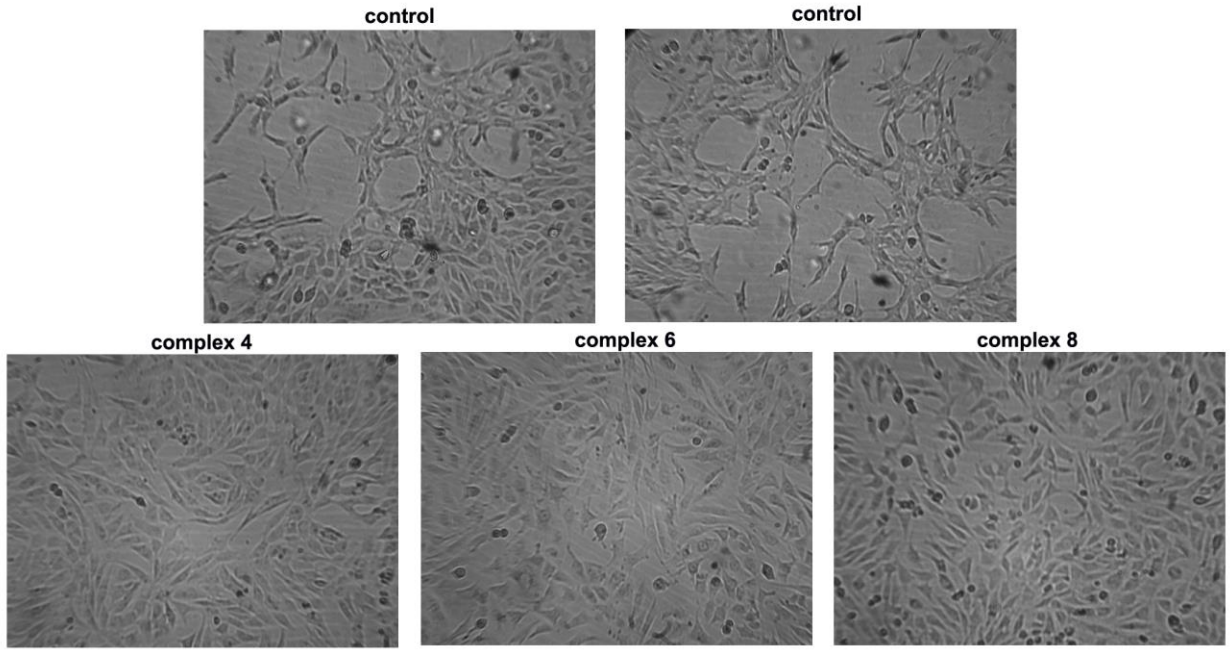

Figure 6. Photomicrographs of control EA.hy926 cells and EA.hy926 cells exposed to sub-toxic IC_{20} concentrations of the complexes **4**, **6** and **8** (200 μM, 50 μM and 50 μM respectively) for 20 h.

3.12. DNA binding studies

DNA is one of the main targets of anticancer agents and it is well established that such compounds can bind to DNA via both covalent and/or non-covalent interactions. For example, cisplatin binds to DNA through covalent bonding via chloride ligand exchange by a nitrogen

containing guanine base of DNA [45]. Non-covalent interactions include intercalation of a planar aromatic moiety between two base pairs of DNA via π-stacking, binding to the minor and major grooves of DNA, and electrostatic interactions with the negatively charged phosphate backbone [46,47]. In this work, spectrophotometric methods were employed to ascertain the interaction modes of **4**, **6** and **8** with CT-DNA. The absorption spectra of complexes **4**, **6** and **8** (Figure 7, Panels A, B and C, black lines) exhibit intense absorption bands at about 300 nm and a shoulder at 340–380 nm. These bands were unperturbed by the presence of CT-DNA (Figure 7, Panels A, B and C, red lines). The observed increase occurring below 300 nm, attributable to DNA absorption, shows that interactions between the complexes and double helix exist, accompanied by hyperchromism, the value of which reached -9.9%, -16% and -7% for **4**, **6** and **8**, respectively. The percentage of hyperchromism was determined from $\{[(\varepsilon_{DNA} + \varepsilon_{COMP}) - \varepsilon_B]/ (\varepsilon_{DNA} + \varepsilon_{COMP})\}$ x 100 where ε_{DNA} is the extinction coefficient of CT-DNA, ε_{COMP} is the extinction coefficient of free metal complex and ε_B is the extinction coefficient of the bound metal complex. The observed negative values for hyperchromism result from possible electrostatic interaction between complex cation and the negatively charged phosphate backbone of DNA molecule.

In order to obtain information on stability of the newly formed complexes **4**/CT-DNA, **6**/CT-DNA and **8**/CT-DNA, spectroscopic titrations of the solutions of CT-DNA were performed. The absorbance at 259 nm was monitored for each concentration of DNA (Figure 7, Panels D, E and F). The binding constant K_b was determined using equation (1) (see Experimental Section). The intrinsic binding constants K_b of the complex **4** (Inset in Figure 7, Panel D) and of the complex **6** (Inset in Figure 7, Panel E) were calculated as 1.29×10^3 M^{-1} and 6.4×10^2 M^{-1}, respectively. The complexes exhibit similar binding affinity towards DNA. Considering that the values differ from the values described in the literature for classical intercalators, for example, ethidium─DNA, 7×10^7 M^{-1} it can be concluded that both complexes bind to DNA *via* the non-intercalative mode. In the case of complex **8** (Inset in Figure 7, Panel F), deviation from linearity might be consequence of other processes such as base modification and/or nicks formation.

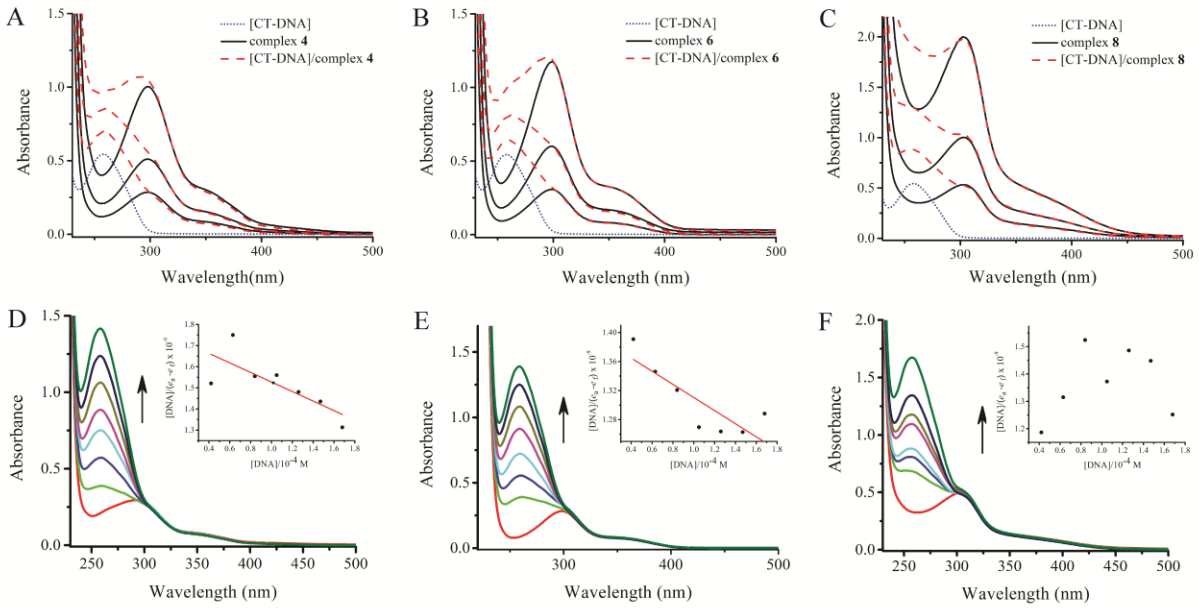

Figure 7. Changes in electronic absorption spectra of the complexes **4** (A), **6** (B) and **8** (C) (1, 2 and 4 × 10^{-5}M) after interactions with CT-DNA (8.4 × 10^{-5} M) and determination of binding constants by absorption titration of **4** (D), **6** (E) and **8** (F) at fixed concentration (1 × 10^{-5} M) with increasing concentrations of CT-DNA (2.1, 4.2, 6.3, 8.4, 10.5, 12.6, 14.7 and 16.8 × 10^{-5} M). The arrows show the changes in absorbance upon increasing amounts of CT-DNA. The insets show the linear fit of [DNA]/(ε_a – ε_f) *vs.* [DNA] and the binding constant (K_b) was calculated using eqn. (1).

To further clarify the nature of interactions of the complexes with CT-DNA, a displacement study was performed. It is known that ethidium bromide (EB) emits intense fluorescent light in the presence of DNA due to its strong intercalation between adjacent base pairs. The extent of fluorescence quenching of EB by competitive displacement from DNA is a measure of the strength of interactions between the second molecule and DNA [48]. The emission spectra of EB bound to CT-DNA in the absence and the presence of **4**, **6** and **8** are shown in Figure 8, Panels A, B and C, respectively. Binding of EB to CT-DNA was evaluated by excitation at 500 nm with maximum fluorescence at 600 nm. The fluorescence intensity of the band at 600 nm of EB─CT-DNA system decreased remarkably with the increasing concentration of the complex compounds. The maximal decrease of EB─CT-DNA fluorescence intensity was about 47 %, by

4 (Figure 8, Panel A), 41.5 % by **6** (Figure 8, Panel B) and about 46 % by **8** (Figure 8, Panel C), suggesting that the three complexes competed with EB in binding to DNA to a similar extent.

The obtained fluorescence quenching data were analyzed by eqn. (2) (see Experimental section).

The plots displayed a good linear relationship for the investigated concentration ranges of **4**, **6** and **8**. The quenching constants for **4**, **6** and **8**, were calculated as K= 0.5979, K = 0.5221 and K = 0.5964, respectively. These data indicate the displacement of ethidium bromide from system EB–CT-DNA by the complexes, but in view of UV/Vis absorption spectral results it is most likely not a consequence of intercalation, but of structural changes in DNA arising from electrostatic binding, which reduce the binding affinity of EB [49].

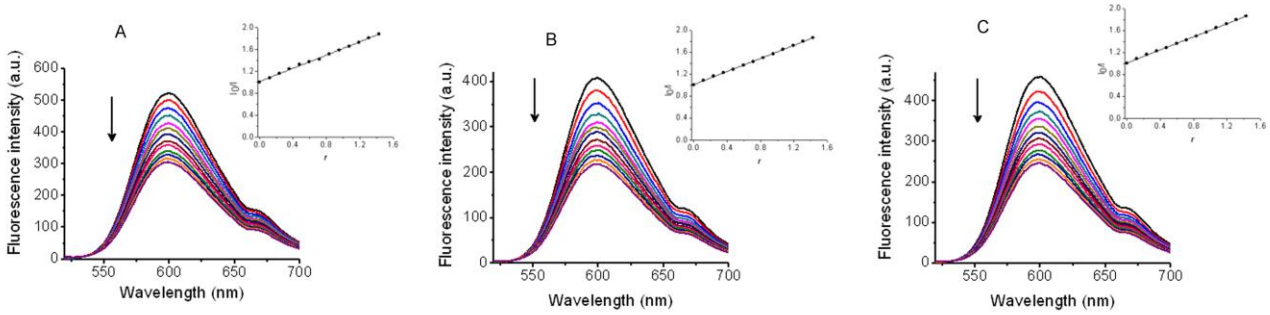

Figure 8. Emission spectra of ethidium bromide (EB) (2.5 x 10^{-5}M) bound to CT-DNA (8.4 × 10^{-5} M) and quenching of EB−CT-DNA system by **4** (Panel A), **6** (Panel B) and **8** (Panel C) at increasing concentrations (1, 2, 3, 4, 5, 6 × 10^{-5} M). The arrows show that fluorescence intensity decreased with increasing concentration of the complex. The insets show fluorescence quenching curves of EB bound to DNA at λ_{max}=600 nm by **4** (Panel A), **6** (Panel B) and **8** (Panel C). The quenching constants K were calculated using eqn. (2) by linear regression of the plot I_0/I against [***r***]/[CT-DNA],where I_0 and I represent the fluorescence intensities of EB−CT-DNA in absence and presence of the complex, and ***r*** = [complex]/[CT-DNA].

To provide additional insight into the interactions between the DNA and the complexes, the study with the minor groove binder Hoechst 33258 was performed.

Hoechst 33258 (H) binds strongly and selectively with high affinity to double-stranded B-DNA structure and like other minor groove binders, it recognizes at least four AT base pairs. It binds by combination of hydrogen bonding, van der Waals contacts with the walls of the minor groove, and electrostatic interactions between its cationic structure and the DNA [50]. Binding of Hoechst 33258 to CT-DNA was followed by excitation at 350 nm with maximum in fluorescence at 444 nm. The fluorescence intensity of the band at 444 nm of the Hoechst−CT-DNA system decreased remarkably with the increasing concentrations of complexes **4**, **6** and **8** (Figure 9, Panels A, B and C, respectively). The maximal decrease of Hoechst−CT-DNA (H–CT-DNA) fluorescence intensity by **4** was 64 %, by **6** 51 % and by **8** 82 %. Results showed that the displacement of Hoechst by the complex **8** was more efficient than by the other two complexes. Insets in Figure 9, Panels A-C show the quenching plots demonstrating the quenching of H bound to CT-DNA by all three complexes are in agreement with the linear Stern-Volmer Eq. (2) for the investigated concentration ranges of **4** (Figure 9, Panel A), **6** (Figure 9, Panel B) and **8** (Figure 9, Panel C). The corresponding quenching constants of H–CT-DNA system by **4**, **6** and **8** were calculated by linear regression of a plot I_0/I against ***r*** as K= 1.238, K = 2.5166 and K = 11.4486, respectively. The complex **8** was the most efficient and some deviation from linearity might be a consequence of stronger electrostatic interaction in a groove of DNA, due to the presence of two mol of complex cation per mole of compound **8**.

DNA binding studies indicate that interactions of the complexes **4**, **6** and **8** with DNA occurred possibly due to electrostatic interactions between a positively charged quaternary ammonium group of the complexes and negatively charged phosphate groups of DNA backbone.

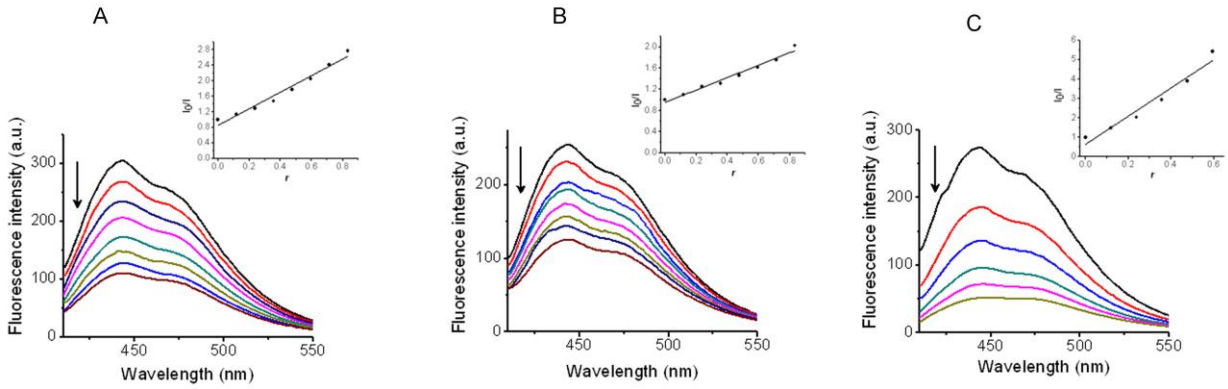

Figure 9. Emission spectra of Hoechst33258 (H) (2.5×10^{-5}M) bound to CT-DNA (8.4×10^{-5}M) and quenching of H−CT-DNA system by **4** (Panel A), **6** (Panel B) and **8** (Panel C) at increasing concentrations (1, 2, 3, 4, 5, 6×10^{-5} M). The arrows show that fluorescence intensity decreased with increasing concentration of the complex. The insets show fluorescence quenching curves of H bound to DNA at λ_{max}=443 nm by **4** (Panel A), **6** (Panel B) and **8** (Panel C). The quenching constants *K* were calculated using eqn. (2) by linear regression of the plot I_0/I against [***r***]/[CT-DNA],where I_0 and I represent the fluorescence intensities of H−CT-DNA in absence and presence of the complex, and ***r*** = [complex]/[CT-DNA].

3.6. DNA cleavage

The type of DNA metal complex interactions has been further established by the investigation of damage to circular DNA. The ability of Co(II), Cd(II) and Fe(III) complexes to cleave double-stranded plasmid pUC19 were investigated using an agarose electrophoretic assay. The assay allows assessment of DNA strand cleavage by monitoring the conversion of untreated supercoiled form (FI) plasmid DNA into the nicked form (FII) and linear form (FIII). As shown in Figure 10 (lanes 1, 7 and 13, panel A; lane 1, panel B), plasmid pUC19 consisted mainly of FI and FII. The addition of increasing concentration of complex **4** to the plasmid resulted in the bands of these plasmid forms smeared in concentration-dependent way. The result indicated that complex **4** has a strong damaging effect, converting DNA to shorter fragments. In the case of **6**, the conversion of forms I and II becomes a much less efficient with increasing concentration of the complex (Figure 10, panel A, lanes 8–12). On the contrary, the strong strand scission activity of Fe(III) complex **8** was obtained. As shown in Figure 10, panel A, lanes 14–18, the interaction of **8** with supercoiled form of pUC19 generated linear FIII form. The increase in the concentration of **8** produced quenching of fluorescence of ethidium bromide in electrophoretic bands. In addition, the formation of the forms with lower mobility became apparent. In the presence of the increasing concentration of free ligand $\mathbf{H_2L}Cl_2$ (Figure 10, panel B, lanes 2–4), changes in intensity and in mobility of supercoiled forms FI and the open circular forms FII of plasmid pUC19 were not observed in comparison to the control (Figure 10, panel B, lane 1). The results indicate that plasmid DNA damage could be consequence of the activity of the redox active complexes **4** and **8**. The effect was most extensive with complex of Co(II) (**4**).

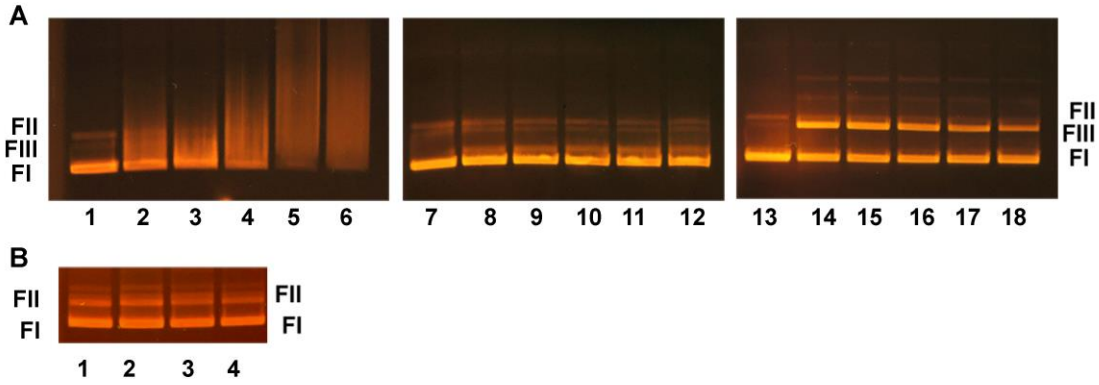

Figure 10. Agarose gel electrophoretic analysis of supercoiled forms FI and the open circular forms FII of plasmid pUC19 (2.6×10^{-9} M) (lanes 1, 7 and 13, panel A; lane 1, panel B) after incubation (1.5 h at 37 °C) with 0.25, 0.5, 1, 1.5 and 2 mM of complex **4**, (lanes 2–6, respectively, panel A); with 0.25, 0.5, 1, 1.5 and 2 mM of complex **6**, (lanes 8–12, respectively, panel A); with 0.25, 0.5, 1, 1.5 and 2 mM of complex **8**, (lanes 14–18, respectively, panel A) and with 0.25, 1 and 2 mM of ligand **H_2L**Cl_2 (lanes 2–4, respectively, panel B).

4. Conclusion

Two newly synthesized cationic complexes as well as six previously synthesized with the same ligand, having the same pentagonal-bipyramidal geometry, showed moderate to low cytotoxic activities towards five tested human cancer cell lines, while the ligand was inactive. Manganese, nickel and zinc complexes showed low activity. Cadmium complex was moderately active towards MDA-MB-453 breast carcinoma cell line, HeLa cervical carcinoma cell line, K562 leukemia cell line and A549 lung carcinoma cell line. Considering two cobalt complexes, the nature of anion influenced the activity – complex **4** with complex tetraisothiocyanatocobaltate(II) anion exerted higher cytotoxic activity on tested malignant cell lines, K562 cells were the most sensitive to the activity of this complex. Iron complex **8** with complex anion $[Fe(H_2O)(NCS)_5]$ exhibited higher intensity of cytotoxic activity than iron complex **7**, with free thiocyanate anion, but in this case, if the results are recalculated for concentration of the complex cation, the effects are opposite. The investigated complexes **4**, and in particular **6** induced alterations in cell cycle phase distribution of HeLa and K562 cells. Cadmium complex **6** caused significant increase of apoptotic subG1 cells in both cell lines. Iron complex **8** induced significant changes in cell cycle

phase distribution only in HeLa cells. Morphological changes in HeLa cells were also indicative of apoptosis, with complex **6** having again the most pronounced effect. Identification of target caspases in HeLa cells showed that complexes **4** and **8** trigger extrinsic and intrinsic apoptotic signaling pathways, while complex **6** exerts effects through intrinsic apoptotic pathway, but also possibly through caspase-independent apoptosis or other cell death types. Complexes **4**, **6** and **8** bind to DNA, most probably by electrostatic interactions, and perturb DNA structure, causing displacement of both ethidium bromide and Hoechst 33258. Complexes **4** and **8** cause cleavage of plasmid DNA in vitro, while cadmium complex **6** is much less efficient. Cleavage of DNA could be provoked by redox activity of complexes **4** and **8** where cobalt and iron are also involved in the complex anion. Complexes **4**, **6** and **8** also showed a weak antiangiogenic effect. Iron (III) complexes **7** and **8** showed a better antimicrobial activity than complexes of other metals with this ligand. It is clear the factors that affect certain type of biological activity of studied compounds are very complex. Without any doubt type of metal ion is very important however, complex anion can also affect results substantially and more studies are needed to better understand all these processes.

Acknowledgements

This work was supported by the Ministry of Education, Science and Technological development of the Republic of Serbia (Grant OI 172055 and Grant OI 175011) and Slovenian Research Agency (P-0175). We thank the EN-FIST Centre of Excellence, Ljubljana, Slovenia, for use of the SuperNova diffractometer.

References

[1] L.D. Popov, A.N. Morozov, I.N. Shcherbakov, Yu.P. Tupolova, V.V. Lukov, V.A. Kogan, Metal complexes with polyfunctional ligands based of bis(hydrazones) of dicarbonyl compounds, Russ. Chem. Rev. 78 (2009) 643–658.

[2] S. Naskar, M. Corbella, A.J. Blake, S.K. Chattopadhyay, Versatility of 2,6-diacetylpyridine (dap) hydrazones in generating varied molecular architectures: Synthesis and structural

characterization of a binuclear double helical Zn(II) complex and a Mn(II) coordination polymer, Dalton Trans. (2007) 1150–1159.

[3] B.A.D. Neto, B.F.L. Viana, T.S. Rodrigues, P.M. Lalli, M.N. Eberlin, W.A. da Silva, H.C.B. de Oliveira, C.C. Gatto, Condensed, solution and gas phase behaviour of mono- and dinuclear 2,6-diacetylpyridine (dap) hydrazone copper complexes probed by X-ray, mass spectrometry and theoretical calculations, Dalton Trans. 42 (2013) 11497–11506.

[4] L.J. Batchelor, M. Sangalli, R. Guillot, N. Guihéry, R. Maurice, F. Tuna, T. Mallah, Pentanuclear Cyanide-Bridged Complexes Based on Highly Anisotropic CoII Seven-Coordinate Building Blocks: Synthesis, Structure, and Magnetic Behavior, Inorg. Chem. 50 (2011) 12045−12052.

[5] S. Naskar, D. Mishra, S.K. Chattopadhyay, M. Corbella, A.J. Blake, Versatility of 2,6-diacetylpyridine (dap) hydrazones in stabilizing uncommon coordination geometries of Mn(II): synthesis, spectroscopic, magnetic and structural characterization, Dalton Trans. (2005) 2428–2435.

[6] F.B. Tamboura, P.M. Haba, M. Gaye, A.S. Sall, A.H. Barry, T. Jouini, Structural studies of bis-(2,6-diacetylpyridine-bis-(phenylhydrazone)) and X-ray structure of its Y(III), Pr(III), Sm(III) and Er(III) complex, Polyhedron 23 (2004) 1191–1197.

[7] R.C. Palenik, K.A. Abboud, S.P. Summers, L.L. Reitfort, G.J. Palenik, Syntheses, crystal structures, and bond valence sum analyses of lanthanide complexes with a planar pentadentate ligand, Inorg. Chim. Acta 359 (2006) 4645–4650.

[8] M. Kozłowski, R. Kierzek, M. Kubicki, W. Radecka-Paryzek. Metal-promoted synthesis, characterization, crystal structure and RNA cleavage ability of 2,6-diacetylpyridine bis(2-aminobenzoylhydrazone) lanthanide complexes, J. Inorg. Biochem. 126 (2013) 38–45.

[9] K. Nomiya, K. Sekino, M. Ishikawa, A. Honda, M. Yokoyama, N.C. Kasuga, H. Yokoyama, S. Nakano, K. Onodera, Syntheses, crystal structures and antimicrobial activities of monomeric 8-coordinate, and dimeric and monomeric 7-coordinate bismuth(III) complexes with tridentate and pentadentate thiosemicarbazones and pentadentate semicarbazone ligands, J. Inorg. Biochem. 98 (2004) 601–615.

[10] P. Mazza, M. Orcesi, C. Pelizzi, G. Pelizzi, G. Predieri, F. Zani, Synthesis, Structure, Antimicrobial, and Genotoxic Activities of Organotin Compounds with 2,6-Diacetylpyridine Nicotinoyl and Isonicotinoylhydrazones, J. Inorg. Biochem. 48 (1992) 251–270.

[11] K.S.O. Ferraz, N.F. Silva, J.G. da Silva, L.F. de Miranda, C.F.D. Romeiro, E.M. Souza-Fagundes, I.C. Mendes, H. Beraldo, Investigation on the pharmacological profile of 2,6-diacetylpyridine bis(benzoylhydrazone) derivatives and their antimony(III) and bismuth(III) complexes, Eur. J. Med. Chem. 53 (2012) 98–106.

[12] I. Ivanović-Burmazović, K. Andjelković, Transition metal complexes with bis(hydrazone)ligands of 2,6-diacetylpyridine. Hepta-coordination of 3d metals, Adv. Inorg. Chem. 55 (2004) 315–360.

[13] N.C. Kasuga, K. Sekino, M. Ishikawa, A. Honda, M. Yokoyama, S. Nakano, N. Shimada, C. Koumo, K. Nomiya, Synthesis, structural characterization and antimicrobial activities of 12 zinc(II) complexes with four thiosemicarbazone and two semicarbazone ligands, J. Inorg. Biochem. 96 (2003) 298–310.

[14] G.F. Liu, M. Filipović, F.W. Heinemann, I. Ivanović-Burmazović, Seven-Coordinate Iron and Manganese Complexes with Acyclic and Rigid Pentadentate Chelates and Their Superoxide Dismutase Activity, Inorg. Chem. 46 (2007) 8825–8835.

[15] C.T. Gutman, T.C. Brunold, Spectroscopic and Computational Studies of a Small-Molecule Functional Mimic of Iron Superoxide Dismutase, Iron 2,6-Diacetylpyridinebis(semioxamazide), Inorg. Chem. 51 (2012) 12729–12737.

[16] C.T. Gutman, I.A. Guzei, T.C. Brunold, Structural, Spectroscopic, and Computational Characterization of the Azide Adduct of FeIII(2,6-diacetylpyridinebis(semioxamazide)), a Functional Analogue of Iron Superoxide Dismutase, Inorg. Chem. 52 (2013) 8909–8918.

[17] C. Gökçe, N. Dilek, R. Gup, Seven coordinated cobalt(II) complexes with 2,6-diacetylpyridine bis(4-acylhydrazone) ligands: Synthesis, characterization, DNA-binding and nuclease activity, Inorg. Chim. Acta 432 (2015) 213–220.

[18] R. Gup, C. Gökçe, N. Dilek, Seven-coordinated cobalt(II) complexes with 2,6-diacetylpyridine bis(4-hydroxybenzoylhydrazone): synthesis, characterisation, DNA binding and cleavage properties, Supramol. Chem. 27 (2015) 629–641.

[19] L.S. Vojinović-Ješić, V.I. Češljević, G.A. Bogdanović, V.M. Leovac, K. Mészáros Szécsényi, V. Divjaković, M.D. Joksović, Transition metal complexes with Girard reagent-based ligands. Part V. Synthesis, characterization and crystal structure of pentagonal-bipyramidal manganese(II) complex with 2,6-diacetylpyridine bis(Girard-T hydrazone), Inorg. Chem. Commun. 13 (2010) 1085–1088.

[20] G. Brađan, B. Čobeljić, A. Pevec, I. Turel, M. Milenković, D. Radanović, M. Šumar-Ristović, K. Adaila, M. Milenković, K. Anđelković, Synthesis, characterization and antimicrobial activity of pentagonal-bipyramidal isothiocyanato Co(II) and Ni(II) complexes with 2,6-diacetylpyridine bis(trimethylammoniumacetohydrazone), J. Coord. Chem. 69 (2016) 801–811.

[21] G. Brađan, A. Pevec, I. Turel, I.N. Shcherbakov, M. Milenković, M. Milenković, D. Radanović, B. Čobeljić, K. Anđelković, Synthesis, characterization, DFT calculations and antimicrobial activity of pentagonal-bipyramidal Zn(II) and Cd(II) complexes with 2,6-diacetylpyridine-bis(trimethylammoniumacetohydrazone), J. Coord. Chem. 69 (2016) 2754–2765.

[22] Oxford Diffraction, CrysAlis PRO, Oxford Diffraction Ltd., Yarnton, England, 2009.

[23] A. Altomare, G. Cascarano, C. Giacovazzo, A. Guagliardi, Completion and Refinement of Crystal Structures with SIR92, J. Appl. Crystallogr. 26 (1993) 343–350.

[24] G. M. Sheldrick, A short history of SHELX, Acta. Crystallogr. Sect. A64 (2008) 112–122.

[25] Clinical and Laboratory Standards Institute (CLSI) 2014. Performance standards for antimicrobial susceptibility testing, 24th Informational Supplement. Approved Standard. CLSI document M100-S24. Wayne, PA, USA.

[26] I.Z. Matić, I. Aljančić, Ž. Žižak, V. Vajs, M. Jadranin, S. Milosavljević, Z.D. Juranić, *In vitro* antitumor actions of extracts from endemic plant *Helichrysum zivojinii*, BMC. Complement. Altern. Med. 13 (2013) 36.

[27] T. Mosmann, Rapid colorimetric assay for cellular growth and survival: application to proliferation and cytotoxicity assays, J. Immunol. Methods. 65 (1983) 55–63.

[28] M. Ohno M, T. Abe, Rapid colorimetric assay for the quantification of leukemia inhibitory factor (LIF) and interleukin-6 (IL-6), J. Immunol. Methods. 145 (1991) 199–203.

[29] M.G. Ormerod. Flow Cytometry. A Practical Approach. Oxford, UK: Oxford University Press, 2000.

[30] E. Aranda, G.I. Owen, A semi-quantitative assay to screen for angiogenic compounds and compounds with angiogenic potential using the EA.hy926 endothelial cell line, Biol Res. 42(2009) 377–389.

[31] I.Z. Matić, I. Aljančić, V. Vajs, M. Jadranin, N. Gligorijević, S. Milosavljević, Z.D. Juranić, Cancer-suppressive potential of extracts of endemic plant *Helichrysum zivojinii*: effects on cell migration, invasion and angiogenesis, Nat. Prod. Commun. 8 (2013) 1291–1296.

[32] M.E. Reichmann, S.A. Rice, C.A. Thomas, P. Doty, A further examination of the molecular weight and size of desoxypentose nucleic acid, J. Am. Chem. Soc. 76 (1954) 3047–3053.

[33] R. Vijayalakshmi, M. Kanthimathi, V. Subramanian, B. Unni Nair, DNA Cleavage by a Chromium(III) Complex, Biochem. Biophys. Res. Commun. 271 (2000) 731–734.

[34] J.R. Lakowicz, G. Weber, Quenching of fluorescence by oxygen. A probe for structural fluctuations in macromolecules, Biochemistry 12 (1973) 4161–4170.

[35] J. Sambrook, E.F. Fritsch, T. Maniatis, In: Molecular Cloning A laboratory manual, 2nd ed., Cold Spring Harbor Laboratory Press, USA, 1989.

[36] W.J. Geary. The use of conductivity measurements in organic solvents for the characterisation of coordination compounds, Coord. Chem. Rev. 7 (1971) 81–121.

[37] K. Andjelković, A. Bacchi, G. Pelizzi, D. Jeremić, I. Ivanović-Burmazović, An Fe(III) Complex with the Dianionic form of 2,6-Diacetylpyridine Bis(Acylhydrazone). The Crystal Structure of [Diaqua-2′,2‴-(2,6-PyridinediyldiEthylidyne)Dioxamohydrazide]Iron(III) Perchlorate Trihydrate, $[Fe(dapsox)(H_2O)_2]ClO_4 \cdot 3H_2O$, J. Coord. Chem. 55 (2002) 1385–1392.

[38] K. Nakamoto, Infrared and Raman Spectra of Inorganic and Coordination Compounds, fourth ed., Wiley-Interscience, New York, 1986, p 283.

[39] X.-L. Li, Z.-S. Lu, D.-Z. Niu, Bis(4-carboxypyridinium)aquapentakis(isothiocyanato-κN)iron(III) bis-(pyridinium-4-carboxylate), Acta Crystallogr. Sect. E, 63 (2007) m2640.

[40] Search of CSD version 5.37 (November 2015) plus one update (May 2016) were conducted using the CONQUEST software.

[41] J.D. Chandler, B.J. Day, THIOCYANATE: A potentially useful therapeutic agent with host defense and antioxidant properties, Biochem. Pharmacol. 84 (2012) 1381–1387.

[42] A.A. Christy, P.K. Egeberg, Oxidation of thiocyanate by hydrogen peroxide — a reaction kinetic study by capillary electrophoresis, Talanta 51 (2000) 1049–1058.

[43] R.H. Betts, F.S. Dainton, Electron Transfer and Other Processes Involved in the Spontaneous Bleaching of Acidified Aqueous Solutions of Ferric Thiocyanate, J. Am. Chem. Soc. 75 (1953) 5721–5727.

[44] E. Brillas, I. Sirés, M.A. Oturan, Electro-Fenton Process and Related Electrochemical Technologies Based on Fenton's Reaction Chemistry, Chem. Rev. 109 (2009) 6570–6631.

[45] S.E. Sherman, D. Gibson, A.H.J. Wang, S.J. Lippard, Crystal and molecular structure of cis-[$Pt(NH_3)_2$[d(pGpG)]], the principal adduct formed by cis-diamminedichloroplatinum(II) with DNA, J. Am. Chem. Soc. 110 (1988) 7368–7381.

[46] L. Strekowski, B. Wilson, Noncovalent interactions with DNA: an overview, Mut. Res. 623 (2007) 3–13.

[47] F.R. Keene, J.A. Smith, J.G. Collins, Metal complexes as structure-selective binding agents for nucleic acids, Coord. Chem. Rev. 253 (2009) 2021–2053.

[48] M. Lee, A.L. Rhodes, M.D. Wyatt, S. Forrow, J.A. Hartley, GC Base Sequence Recognition by Oligo(imidazolecarboxamide) and C-Terminus-Modified Analogues of Distamycin Deduced from Circular Dichroism, Proton Nuclear Magnetic Resonance, and Methidiumpropylethylenediaminetetraacetate-Iron(II) Footprinting Studies, Biochemistry. 32 (1993) 4237–4245.

[49] C.B. Spillane, J.A. Smith, J.L. Morgan, F.R. Keene, DNA affinity binding studies using a fluorescent dye displacement technique: the dichotomy of the binding site, J. Biol. Inorg. Chem. 12 (2007) 819–824.

[50] R. Kakkar, R. Garg, Suruchi, Towards understanding the molecular recognition process in Hoechst–DNA complexes, J. Mol. Struct. 584 (2002) 37–44.

Synopsis

Pentagonal-bipyramidal Fe(III) complexes with dihydrazone of 2,6-diacetylpyridine and Girard's T reagent have been synthesized and characterized. Cytotoxic activity of Fe(III) complexes and Co(II), Ni(II), Mn(II), Zn(II) and Cd(II) complexes with the same ligand was tested. The best activity was observed in the case of Fe(III), Co(II) and Cd(II) complexes.

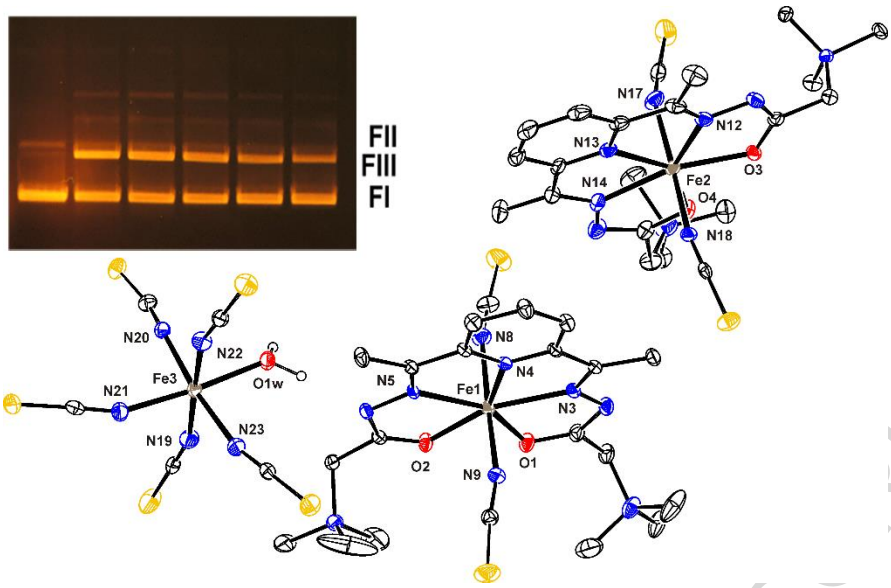

Graphical abstract

Highlights

- pentagonal-bipyramidal Fe(III) complexes
- cytotoxic activity
- effect on cell cycle progression in tumor cells
- DNA interactions